THE JOURNAL OF BIOLOGICAL CHEMISTRY VOL. 291, NO. 3, pp. 1529–1537, January 15, 2016

MicroRNA-424 Predicts a Role for β-1,4 Branched Glycosylation in Cell Cycle Progression*

Received for publication, June 17, 2015, and in revised form, October 27, 2015 Published, JBC Papers in Press, November 20, 2015, DOI 10.1074/jbc.M115.672220

Christopher A. Vaiana[1], **Tomasz Kurcon, and Lara K. Mahal**[2]

From the Biomedical Chemistry Institute, Department of Chemistry, New York University, New York, New York 10003

MicroRNA regulation of protein expression plays an important role in mediating many cellular processes, from cell proliferation to cell death. The human microRNA miR-424 is up-regulated in response to anti-proliferative cytokines, such as transforming growth factor β (TGFβ), and directly represses cell cycle progression. Our laboratory recently established that microRNA can be used as a proxy to identify biological roles of glycosylation enzymes (glycogenes). Herein we identify MGAT4A, OGT, and GALNT13 as targets of miR-424. We demonstrate that MGAT4A, an *N*-acetylglucosaminyltransferase that installs the β-1,4 branch of *N*-glycans, is directly regulated by miR-424 in multiple mammary epithelial cell lines and observe the loss of MGAT4A in response to TGFβ, an inducer of miR-424. Knockdown of MGAT4A induces cell cycle arrest through decreasing CCND1 levels. MGAT4A does not affect levels of β-1,6 branched *N*-glycans, arguing that this effect is specific to β-1,4 branching and not due to gross changes in overall *N*-linked glycosylation. This work provides insight into the regulation of cell cycle progression by specific *N*-glycan branching patterns.

The central dogma of molecular biology defines the major direction of information flow from DNA to RNA to protein (1). However, the last few decades of research has led us to realize that additional information is encoded in RNA-RNA interactions and posttranslational modifications (2, 3). MicroRNA (miRNA),[3] small non-coding RNA sequences (~22 nucleotides), have been heralded as regulators of gene expression that control posttranscriptional mRNA stability or translation (4, 5). miRNAs tune out transcriptional noise, allowing tighter control over protein expression of critical proteins defining a cell (6). Much like miRNA, glycosylation has the ability to exert global regulatory effects within the cell and its surroundings, and dysregulation can lead to biological disorders (7). Recent work by our laboratory has shown that miRNAs are important regulators of glycosylation (8) and can be used as a proxy to define the biological functions of glycosylation enzymes (9).

The human miRNA hsa-miR-424-5p (miR-424), a member of the miR-15 family, plays a role in cell cycle regulation (10, 11). miR-424 is a critical component of mammary gland involution in the breast in response to TGFβ (12, 13). Recent findings show that increased miR-424 mediates cell cycle arrest in mammary epithelial cells. It does so by directly targeting and suppressing cyclin-D1 (CCND1) and the phosphatase CDC25A, promoters of G_1 to S phase progression (13, 14). This suggests that glycosylation enzymes targeted by miR-424 regulate cell proliferation.

Glycosylation influences nearly all cellular processes (15). Both *N*-glycan branching and the nucleocytoplasmic *O*-linked *N*-acetylglucosamine (*O*-GlcNAc) have been shown to play roles in cell growth (16–19). Metabolic UDP-GlcNAc levels drive increased *N*-glycan branching that stimulates growth at lower levels and leads to cell cycle arrest at high concentrations via attenuation of TGFβ/SMAD signaling (18). This regulation is thought to occur in part through changes in the binding of galectin-3, an *N*-acetyllactosamine binding lectin that forms cell surface glycan/lectin lattices altering growth factor signaling (20). Changes in *O*-GlcNAc levels also influence cell cycle progression (17). For example, *O*-GlcNAc transferase (OGT) is concentrated at the mitotic spindle and plays a role in chromatin dynamics (17, 21).

In this study we examine three predicted glycogene targets of miR-424: MGAT4A, OGT, and GALNT13. MGAT4A (mannosyl(α-1,3-)-glycoprotein-β-1,4-N-acetylglucosaminyltransferase, isozyme A) is responsible for installing the β-1,4 branch on complex *N*-glycans, whereas GALNT13 is one of 20 enzymes known to initiate canonical *O*-glycosylation. Although luciferase assays confirm all three as miR-424 targets, only MGAT4A is significantly altered in response to miR-424 in breast cell lines. Induction of miR-424 by the anti-proliferative cytokine TGFβ correlated with loss of MGAT4A. Knockdown of MGAT4A inhibited cell proliferation and decreased CCND1 levels. No significant change in β-1,6 branching is observed in MGAT4A knockdown cells, suggesting that these effects on cell cycle progression are not due to a general loss of *N*-glycan branching but rather the manipulation of specific branching patterns.

Experimental Procedures

Cell Lines, miRNA Transfection, and shRNA Conditions—MCF-7 and MDA-MB-231 cells were obtained from the Division of Cancer Treatment and Diagnosis Tumor Repository (National Cancer Institute, Frederick, MD) and cultured in

* The authors declare that they have no conflicts of interest with the contents of this article.

[1] Supported by a Margaret Strauss Kramer Fellowship, New York University.
[2] Supported by the Sokol Foundation. To whom correspondence should be addressed: Dept. of Chemistry, New York University, 100 Washington Square East Rm. 1001, New York, NY. Tel.: 212-998-3533; Fax: 212-995-4475; Email: lkmahal@nyu.edu.

[3] The abbreviations used are: miRNA, microRNA; CCND1, cyclin D1; *O*-GlcNAc, *O*-linked *N*-acetylglucosamine; OGT, *O*-GlcNAc transferase; MGAT4A, mannosyl(α-1,3-)-glycoprotein-β-1,4-*N*-acetylglucosaminyltransferase, isozyme A; GALNT3, polypeptide *N*-acetylgalactosaminyltransferase 3; HBSS, Hanks' buffered saline solution; qRT-PCR, quantitative real-time PCR; NTC, non-targeting control.

TABLE 1

Primers used for 3′-UTR luciferase constructs

Primers used for the generation of the 3′-UTR luciferase constructs. [P], 5′-phosphorylated.

Construct	Forward primer	Reverse primer
MGAT4A	ATATGCTAGCGGTAGAGGGGGCTGC	ATACTCGAGCACCTATTTTTATTAGAAGGAATC
MGAT4A_M1	[P]CTAGTAACTGGTCCTGTTGATTG	[P]GTTTTCAATTATATCTGTATATCTGAAAATAAATAATC
MGAT4A_M2	[P]GGTGTTTTAACCAGGTTAATTTGTGGC	[P]ACTGATTTATTATCTCATAGTTC
MGAT4A_M3	[P]CTGAGCCTTAATAAGCCAGGTTTCGACAGTACTG	[P]AGAATATGTCTTCAAAAGATATTTTCACC
OGT	TTGCTAGCCACATGATTAAGCCTGTTGAAGT	AATGGATCCCAAAATACATCAGCCGTATTA
OGT_M	[P]GACTGCCCCCTCTAAGATACCTCCAAAAGTGAT	[P]GGTAAAACACTGGTGAAACAGGTCAAAA
GALNT13	ATATGCTAGCCTTGGGCACATGAAGATC	ATACTCGAGAATATAGCAGCATTTTAATAAAATTTC

EMEM (minimum essential medium with Earle's salts; MCF-7, Lonza) or RPMI 1640 (MDA-MB-231, Lonza) supplemented with 10% fetal bovine serum (FBS, v/v, Innovative Research). HEK 293/T17 cells (ATCC) were cultured in DMEM (Lonza) supplemented with 10% FBS. HMLE cells were obtained from Robert A. Weinberg (Massachusetts Institute of Technology) and cultured in 1:1 DMEM:F-12 medium supplemented with 10 ng/ml human EGF, 0.5 μg/ml hydrocortisone, 10 μg/ml insulin, and penicillin/streptomycin as previously described (22). All cells were cultured at 37 °C in 5% CO_2.

For miRNA experiments, 1×10^5 cells were transfected with 50 nM concentrations of either mimics or inhibitors (miR-424 and scrambled controls; Dharmacon/GE Healthcare) in Lipofectamine 2000 (1 ml total volume, Life Technologies) and plated in a single well of a 12-well tissue culture dish. After 48 h, cells were harvested with 0.25% trypsin-EDTA (200 μl, Corning) after which 1 ml of medium was added to quench the trypsin. Cells were pelleted (10,000 $\times$ *g*, 4 °C) and washed 1$\times$ in HBSS (Hank's buffered saline solution), and the pellet was snap-frozen in liquid N_2 for further analysis.

To generate shRNA knockdowns of MGAT4A, MISSION shRNA clones (TRCN000035813 (KD-1) and TRCN0000 035812 (KD-2)) or non-targeting control (SHC016, Sigma) were obtained as viral stocks from the shRNA Core at New York University Langone Medical Center. MCF-7 or MDA-MB-231 cells were seeded at 5×10^4 cells in a 6-well format and transduced 24 h after plating with the appropriate shRNA lentivectors (multiplicity of infection = 2) in media containing 8 μg/ml Polybrene. After 48 h, the medium was replaced with selection media (MCF-7: 1.5 μg/ml puromycin; MDA-MB-231: 1 μg/ml puromycin), and cells were maintained as stable selected cell lines for up to 5 passages. For protein and RNA, cells were analyzed at passage 1 post-selection. Each cell line was generated in triplicate.

TGFβ Treatment of HMLE Cells—TGFβ treatments were performed as previously described (23). In brief, 6.7×10^5 HMLE cells were seeded in T-25 culture flasks and grown under standard conditions for 24 h; medium was then replaced with 10 ml of DMEM:F-12 containing 5% calf serum (HyClone) and either 5 ng/ml TGFβ or vehicle (1 mg/ml BSA in 4 mM HCl; TGFβ reconstitution buffer). At 48 h post-treatment, cells were harvested with 0.25% trypsin-EDTA and pelleted as before for further analysis.

Luciferase Reporter Assay—The 3′-UTRs of MGAT4A (NM_001160154), OGT (NM_181672), and GALNT13 (NM_ 052917) were cloned from MCF-7 cDNA using Q5 Hotstart Polymerase (New England BioLabs) and inserted into the pLightSwitch_3′-UTR vector (SwitchGear Genomics) using the primers listed in Table 1. Plasmids were purified using Endo-Free Plasmid Maxi kit (Qiagen). HEK 293/T17 cells (7×10^4) were co-transfected with plasmid (250 ng) and microRNA mimics (60 nM) using Lipofectamine 2000 and plated in a well of a 96-well plate (100 μl total volume). After 24 h, the assay was developed with the LightSwitch Assay Reagent (SwitchGear Genomics), and luminescence was read on a Biotek microplate reader. For each assay we calculated the average -fold change as a ratio miR-424/scramble relative to the treated empty vector for five replicate wells per condition. It should be noted that miR-424 decreases the signal of the empty vector, most likely due to its anti-proliferative effects; thus, we normalized our data to account for this effect. Data presented represent the average of three replicate assays.

Western Blotting—Cell pellets (treated or control) were thawed on ice in cold radioimmune precipitation assay buffer (~100 μl, Sigma) supplemented with protease inhibitors to lyse the cells. Lysates were quantified using the DC assay (Bio-Rad). Equal amounts of protein were resolved by 8% or 10% SDS-PAGE and transferred onto nitrocellulose membranes (Tris-Glycine buffer, 20% methanol, and either 1 h at 350 mA or 16 h at 90 mA). Blots were blocked in 5% (w/v) nonfat milk in TBST (TBS, pH 7.4, 0.05% Tween 20) for 1 h at room temperature. Blots were then incubated with the following primary antibodies for 16 h at 4 °C. Dilution buffers are noted: α-MGAT4A (clone 8C5, Abnova, 1:1000, 5% BSA in TBST); α-galectin-3-biotin (clone M3/38, eBioscience, 1:1000, 5% milk in TBST); α-E-cadherin (clone EP700Y, Abcam, 1:5000, 5% BSA in TBST); α-actin (Thermo Scientific, 1:10,000, 5% milk in TBST). Blots were then washed 3 $\times$ 5 min in TBST after which the corresponding HRP-conjugated secondary antibodies (α-mouse IgG, α-rabbit IgG, Bio-Rad; α-biotin, Cell Signaling) were applied for 1 h at room temperature at a 1:5000 dilution in 5% milk in TBST. Blots were washed 3 $\times$ 5 min TBST and then developed using SuperSignal West Pico (Thermo Scientific).

RNA Extraction and Quantitative Real-time PCR (qRT-PCR)—Cell pellets (treated or control) were thawed, and total RNA was extracted (miRNeasy mini kit; Qiagen). Only cell pellets frozen for 1 week or less were used for RNA extraction. RNA was quantified by using NanoDrop ND-1000 and reverse-transcribed (High Capacity cDNA Reverse Transcription Kit; Applied Biosystems) into cDNA using 750 ng of RNA input. Transcripts were quantified by qRT-PCR using PowerSYBR Green PCR Master mix (Applied Biosystems) in a LightCycler 480 (Roche Applied Science). Primers were designed with qPrimerDepot (primerdepot.nci.nih.gov) and are listed in Table 2. Cycle threshold values were normalized to the β-actin gene ACTB as an internal control. Each run was performed in

TABLE 2
Primers used for qRT-PCR analysis

Gene symbol	Forward primer	Reverse primer
CCND1	TCCTCTCCAAAATGCCAGAG	GGCGGATTGGAAATGAACTT
CDC25A	CAACTAATCCAGAGAAGGCCC	AAGGTCCCTTGGGTCATTGT
GALNT13	TCCTGGTCATCTTTAGGAATCA	AGATCTCTGCTGCCTGCATT
LGALS3	GGGGAAGGGAAGAAAGACAG	TGCAACCTTGAAGTGGTCAG
LGALS1	AGGTTGTTGCTGTCTTTGCC	CAAACCTGGAGAGTGCCTTC
MGAT4A	TCTACCAAGGGCATACGCTGGA	GATGTTCTTGGTTGCCGCTATGG
MGAT4B	TCACTGCCGAAGTGTACTGTG	CTGACACTCTGCACTCGCTC
MGAT5	GTGAGGGTAGCCGTCCATAG	CAGCTTGGTTGCACTTGAGA
OGT	CACTTCCAGTGTCGAAGGCT	GCCAGAAGGGGGTTCTGTTT
SMAD3	TGGACGCAGGTTCTCCAAAC	CCGGCTCGCAGTAGGTAAC
SMAD4	GCTGCAGAGCCCAGTTTAGA	CCCCAAAGCAGAAGCTACGA
TWIST1	CACGCGCGGCTCAGCTACGC	ACAATGACATCTAGGTCTCCGGCCC

triplicate for each gene. The average relative -fold change (set to either non-targeting shRNA or scrambled control) was calculated using the ΔΔCT method (24). Data shown are the average of three biological replicates. *Error bars* represent the S.D.

For miR-424 quantification, the TaqMan Reverse Transcription kit (Applied Biosystems) was used with 10 ng of RNA input followed by the TaqMan microRNA Assay (Applied Biosystems). The miR-424 was then quantified by qRT-PCR as described above.

Cell Cycle Analysis—MCF-7 cells (MGAT4A-KD-1 or control) were harvested as described, washed, and resuspended in 200 μl of cold TBS. Cells were then fixed by the addition of 1 ml of 70% ethanol for 16 h at −20 °C. Before flow cytometry analysis, cells were pelleted (30 min, 10,000 × *g*), the pellet was washed with 1 ml of HBSS, and the washed pellet was resuspended in 500 μl of FxCycle (Life Technologies). Cells were then analyzed using a BD Acuri 6 benchtop flow cytometer (BD Biosciences) by counting 20,000 cells with the FL3A detector. Results were quantified using the univariate cell cycle analysis algorithm (FlowJo). Data shown are the average of three biological replicates.

Cell Proliferation Analysis—MGAT4A knockdown or shRNA control cells were plated in triplicate in a 12-well plate at 50,000 cells/well. A single well was harvested at 24, 48, and 72 h and counted using a hemocytometer. Data presented are the average of three biological replicates at varying cell passages.

Immunofluorescence—MGAT4A knockdown or shRNA control cells were plated on glass-bottom 30-mm dishes (Corning) at 2.5×10^4 cells/cm^2 and cultured for 5 days. The cells were then washed with HBSS (3 × 2 ml, 5 min), fixed with 4% formaldehyde (1.5 ml, 10 min), and permeabilized with 0.2% Triton X (1.5 ml, 5 min). Samples were then blocked with 5% bovine serum albumin in HBSS (2 ml, 30 min) and incubated with primary antibodies or lectins diluted in HBSS as follows for 1 h at room temperature: α-galectin-3 (1:250), α-E-cadherin (1:500), biotinylated-PHA-L (1:500, Vector Laboratories). Cells were then washed with 3 × 1 ml of HBSS and incubated with the appropriate secondary antibodies (streptavidin-Cy5 or α-rabbit IgG-FITC; Sigma) in HBSS at room temperature for 1 h at a 1:1000 dilution. Cells were again washed (3 × 1 ml HBSS) and treated with DAPI (300 nM in HBSS, 5 min), which was removed, and HBSS was added (2 ml) before imaging. Cells were imaged via fluorescence microscopy (40×-PlanFluor objective, NA 0.3, excitation/emission, 625–650 nm/670 nm, Eclipse TE 2000-U; Nikon). Fluorescence images within an experiment were acquired under identical conditions.

TABLE 3
3′ UTR Alignment to miR-424

Name	mirSVR score	Alignment	
	-1.25	G U A C U U A A C G A C G A C A - G A U U U G C U G C U	MiR-424 MGAT4A*
MGAT4A	-0.06	C G A C G A G C U G C U	MiR-424 MGAT4A*
	-0.03	U U A A C G A C G A A A U G G C U G C U	MiR-424 MGAT4A*
OGT	-0.61	A C G A C G A U G C U G C U	MiR-424 OGT*
GALNT13	-1.25	A C G A C G A U G C U G C U	MiR-424 GALNT13

* mutation sites are underlined.

Results

miR-424 Targeted the 3′-UTR of Predicted Glycosyltransferases—We identified MGAT4A, OGT, and GALNT13 as the top three predicted glycogene targets of miR-424 using the summed miRSVR score on the miRanda database (Table 3) (25, 26). For OGT, the mRNA transcript containing the highest prediction score was a truncated product; thus, we examined the 3′-UTR of the full-length gene. To validate these interactions we used a luciferase assay in which the 3′-UTR of our glycogene is appended to a luciferase reporter (Fig. 1*A*). In brief, HEK293/T17 cells were co-transfected with the reporter construct (3′-UTR, mutant or luciferase control) and an miR-424 or scrambled mimic. After 24 h, luminescence readings were obtained. Data are reported as -fold change of miR-424/scrambled treatments normalized to the luciferase controls (Fig. 1*B*). The results confirm that all three genes are targets of miR-424. We validated the predicted binding sites of MGAT4A and OGT by site-directed mutagenesis of the seed regions (Table 3, underlined residues). Mutation of all three predicted miR-424 binding sites in MGAT4A completely abolished miR-424 repression of luciferase. In contrast, mutation of the miR-424 binding site in OGT only partially diminished the repression of the luciferase signal, suggesting the presence of other miR-424 binding sites in the OGT 3′-UTR (Fig. 1*B*). Overall, our data demonstrate that miR-424 can regulate MGAT4A, OGT, and GALNT13 through binding to their 3′-UTRs.

miR-424 Targeted Endogenous MGAT4A in Breast Cell Lines—Next, we examined the effects of miR-424 transfection on the expression of endogenous MGAT4A, OGT, and GALNT13 in the mammary epithelial cancer cell line MCF-7. In brief, MCF-7 cells were transfected with either miR-424 or scrambled mimic (50 nM), and cells were analyzed 48 h post-transfection. Of the three glycosylation enzymes, only MGAT4A showed a significant decrease in mRNA levels by qRT-PCR upon miR-424 treatment ($p < 0.001$, Fig. 1, *C* and *F*). Concomitant with this finding, the protein level of MGAT4A, but not OGT, is seen to decrease by Western blot analysis in miR-424-treated MCF-7 cells (Fig. 1, *D* and *E*). Thus we focused our studies on MGAT4A.

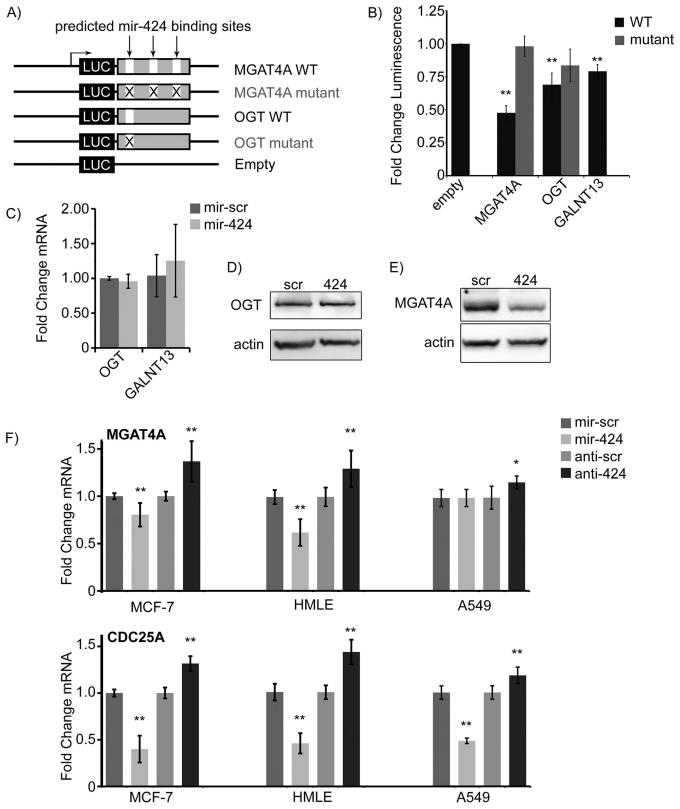

FIGURE 1. **Validation of predicted glycogenes as miR-424 targets.** *A*, schematic depiction of the 3′-UTR luciferase reporter assay and miR-424 binding site mutants. *B*, luciferase assays show MGAT4A, OGT, and GALNT13 are significantly targeted by miR-424. The graph displays average normalized -fold change (mimic/scramble). **, $p < 0.01$, Student's *t* test *versus* empty vector. The *gray bars* represent mutants of appropriate miRNA binding sites (see Table 3). *C*, MCF-7 cells treated with miR-424 mimic did not alter OGT or GALNT13 transcript levels by qRT-PCR. The graph shows -fold change of mRNA ($2^{-\Delta\Delta CT}$) *versus* scramble (*mir-scr*). *D* and *E*, representative Western blot analysis of cells treated as in *C* and probed for OGT and MGAT4A protein. *F*, cell lines (MCF-7, HMLE, A549) were treated with miR-424 mimic or anti-miR, and changes in MGAT4A (*top*) and CDC25A (*bottom*) transcript levels were analyzed by qRT-PCR as previously described. **, $p < 0.01$; *, $p < 0.05$, Student's *t* test *versus* appropriate scrambled control. All experiments were done in biological triplicates. *Error bars* represent the S.D.

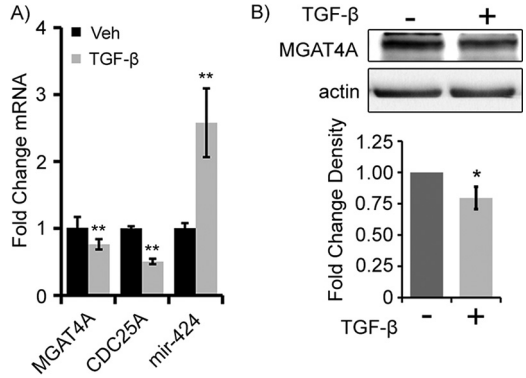

FIGURE 2. **TGFβ induces miR-424 and decreases MGAT4A and CDC25A in HMLE.** *A*, levels of MGAT4A and CDC25A decrease, whereas mature miR-424 increases in HMLE cells treated with 5 ng/ml TGFβ for 48 h by qRT-PCR. The graph shows -fold change of mRNA ($2^{-\Delta\Delta CT}$) *versus* vehicle-treated cells. **, $p < 0.01$ *versus* vehicle-treated control. *B*, representative Western blot analysis of MGAT4A in HMLE cells treated as described (*top*). The graph (*bottom*) represents average -fold change of MGAT4A band density for treated *versus* vehicle-treated control normalized to Ponceau staining in three independent replicates. *, $p < 0.05$. All experiments were done in triplicate. *Error bars* represent the S.D.

We analyzed the impact of miR-424 on MGAT4A levels in three different cell lines: MCF-7; HMLE, a transformed normal breast cell line; A549, a human metastatic lung cell line (Fig. 1*F*). CDC25A, a validated miR-424 target, was used as a positive control. Transfection of miR-424 mimics inhibited MGAT4A expression in both breast cell lines but had no impact in A549. In contrast, CDC25A was inhibited by miR-424 in all cell lines examined. Treatment of the cells with an inhibitor of endogenous miR-424 (anti-424, Fig. 1*F*) increased mRNA levels of MGAT4A in all three cell lines. Taken together these data argue that MGAT4A is a direct target of endogenous miR-424.

TGFβ Induced miR-424 and Decreased Both CDC25A and MGAT4A in HMLE Cells—TGFβ is a potent anti-proliferative cytokine that drives both normal mammary gland morphogenesis (12) and invasive phenotypes in pathogenic cancer cells (27). TGFβ induces miR-424, which subsequently targets CDC25A and CCND1, arresting cell cycle progression (13, 14). With this in mind, we examined regulation of MGAT4A in response to TGFβ in HMLE cells. In brief, HMLE cells were treated with TGFβ (5 ng/ml) or control vehicle for 48 h and were then analyzed for expression of MGAT4A, CDC25A, and miR-424. Levels of endogenous miR-424 increased, in agreement with the previous work (12, 13). In line with these findings, expression of both MGAT4A and CDC25A decreased after 48 h of treatment (Fig. 2). This suggests that MGAT4A levels are controlled by endogenous miR-424 in response to TGFβ.

Loss of MGAT4A Led to Decreased Cell Proliferation and Cell Cycle Arrest—To study whether loss of MGAT4A mimics the effects of miR-424 we generated MGAT4A knockdown cell lines (MGAT4A-KD) in two different breast cancer cells, MCF-7 and MDA-MB-231. In brief, cells were treated with lentiviral vectors containing either MGAT4A shRNA or a non-targeting control (NTC) and selected with puromycin. For MCF-7, we generated knockdowns with two different shRNAs (KD-1, KD-2). The knockdown of MGAT4A in both cell lines was confirmed by qRT-PCR analysis (Fig. 3, *A* and *D*). KD-1 and KD-2 gave similar levels of knockdown of MGAT4A by qRT-PCR (~70%), but KD-1 showed a stronger effect by Western blot analysis (Fig. 3*B*). Although these cells could be cultured, proliferation rates of the MGAT4A-KD cell lines were significantly lower than those of NTC cells for both MCF-7 and MDA-MB-231 (Fig. 3, *C* and *E*). MGAT4A-KD cell lines showed decreased CCND1 expression (MCF-7-KD-1, 30%; MCF-7-KD-2, 50%; MDA-MB-231-KD-1, 42%, compared with NTC, $p < 0.01$; Fig. 3, *A* and *D*). CDC25A expression decreased in MCF-7-MGAT4A-KDs (KD-1, 31%; KD-2, 21%, compared with NTC, $p < 0.01$) but not MDA-MB-231-MGAT4A-KD. These results imply a concomitant change in cell cycle progression.

We next performed flow cytometry analysis on synchronized MCF-7-MGAT4A-KD-1 and control cells to examine more closely changes in cell cycle progression. In brief, cells were starved for 24 h to synchronize their cell cycles. Media containing serum was then added, and cells were analyzed at 0 and 20 h by the method of Crissman and Steinkamp (28). Analysis showed an arrest in the 2N phase for the MGAT4A-KD-1 cells,

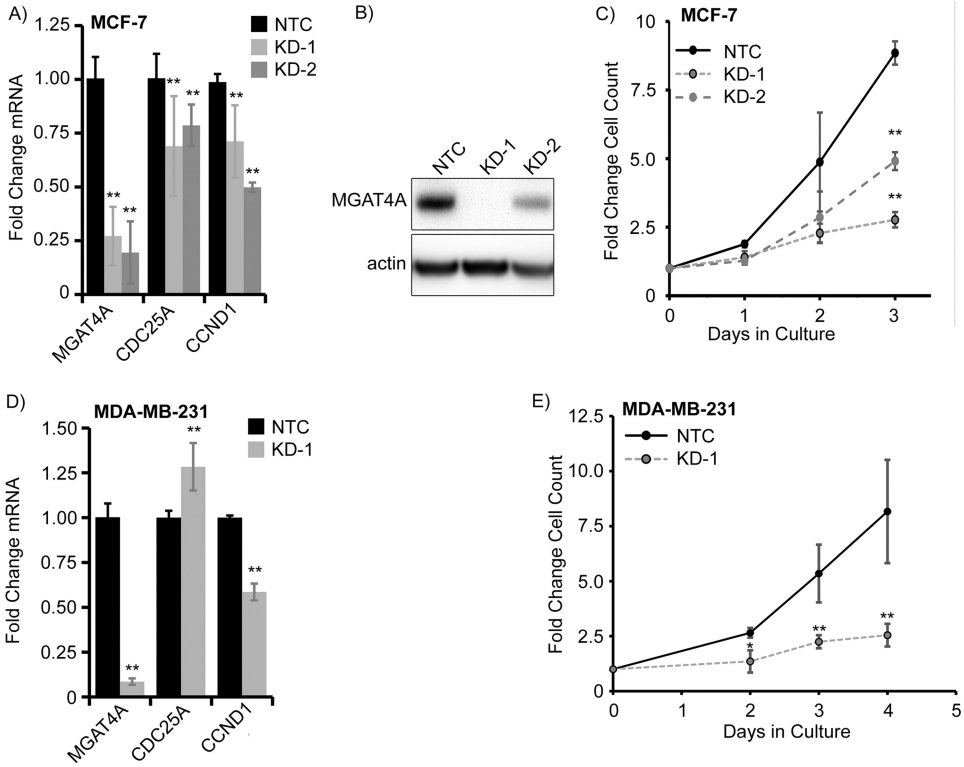

FIGURE 3. **Loss of MGAT4A leads to decreased cell proliferation and cell cycle arrest.** *A*, MGAT4A, CDC25A, and CCND1 levels are significantly reduced in MGAT4A-KD MCF-7 cells. Data for MCF-7 cells independently treated with two different shRNAs (KD-1, KD-2) are shown. The graph shows -fold change of mRNA ($2^{-\Delta\Delta CT}$) *versus* NTC. *B*, representative Western blot analysis of MGAT4A protein levels in MGAT4A-KD MCF-7 cells. *C*, growth curves of MGAT4A-KD cells *versus* NTC. Cell count is shown as -fold change over number of cells plated. *D*, MGAT4A and CCND1 levels are significantly reduced, whereas levels of CDC25A are elevated in MGAT4A-KD MDA-MB-231 cells. Graphs are as previously described in *A*. *E*, growth curve of MDA-MB-231-MGAT4A-KD cells *versus* NTC. Graphs are as previously described in *C*. **, $p < 0.01$; *, $p < 0.05$ *versus* NTC for all graphs. Experiments were done in biological triplicate. *Error bars* represent the S.D.

indicating a reduction in cells transitioning from G_1 to S phase by ~30% (Fig. 4). These results are consistent with previous observations for miR-424 (14) and imply that MGAT4A levels affect cell cycle progression.

Impact of MGAT4A Levels on the Cell Cycle Are Not Due to the Loss of β-1,6 Branched Glycans—The elaboration of biantennary branched *N*-glycans to triantennary requires the addition of GlcNAc to either the C-4 position on the 1,3 mannosyl arm (MGAT4A/B) or to the C-6 position on the 1,6 mannosyl arm (MGAT5) (29). Branching to the tetraantennary then requires the action of the other MGAT enzyme (Fig. 5*A*) (16, 30). Increased *N*-glycan branching has been shown to drive responsiveness to TGFβ signaling leading to growth arrest (18). In the previous study responsiveness correlated with binding by the lectin PHA-L, a known binder of β-1,6 branched *N*-glycans (31). Analysis of glycan microarray data from the Consortium for Functional Glycomics shows that it has no recognition of β-1,4 branched triantennary structures (Fig. 5*B*). To test whether loss of MGAT4A alters β-1,6 branched *N*-glycan production through MGAT5, we examined the transcript levels of all three branching enzymes in MCF-7-MGAT4A-KD-1. As previously discussed, we observed a ~70% decrease in MGAT4A levels; however, no significant compensatory changes in either MGAT4B or MGAT5 were observed (Fig. 5*C*). It should be noted that MGAT4A$^{-/-}$ knock-out mice retain only 2–20% β-1,4 GlcNAc transferase activity (32), and MGAT4B has a lower affinity for both UDP-GlcNAc and substrates (33), arguing that it cannot compensate for loss of MGAT4A activity in our knockdown cells. Staining of MGAT4A-KD cells with PHA-L showed no noticeable changes in PHA-L binding (Fig. 5*D*). Taken together, our data argues that MGAT4A exerts its effects on cell cycle progression independent of β-1,6 branched glycans and implies a specific role for the β-1,4 branch in cell cycle regulation.

Galectin-3 Expression Increases in Response to miR-424 and Loss of MGAT4A in MCF-7—Previous work established galectin-3 as a key mediator between *N*-glycan branching patterns and changes in growth factor signaling that result in altered proliferation (18, 20). Galectin-3 has also been shown to have glycan-independent effects on the cell cycle, halting cell cycle progression at the G_1 phase by regulating transcription factor binding in the nucleus (34, 35). With this in mind, we analyzed galectin-3 levels in response to either miR-424 or MGAT4A-KD in MCF-7 cells. Analysis of miR-424-treated cells showed a significant increase in galectin-3 levels as measured by both qRT-PCR and Western blot analysis (Fig. 6, *A* and *B*). A similar increase was observed in the MGAT4A-KD cells (Fig. 6, *C* and *D*).

Localization of galectin-3 dictates its role, with cell surface galectin-3 causing sensitization of cytokine receptors (20) and nuclear galectin-3 playing a direct role in transcription factor binding (36). We analyzed the cellular localization of galectin-3 in MGAT4A-KD cells by fluorescence microscopy (Fig. 6*E*). We could not observe galectin-3 in NTC cells. Galectin-3 in

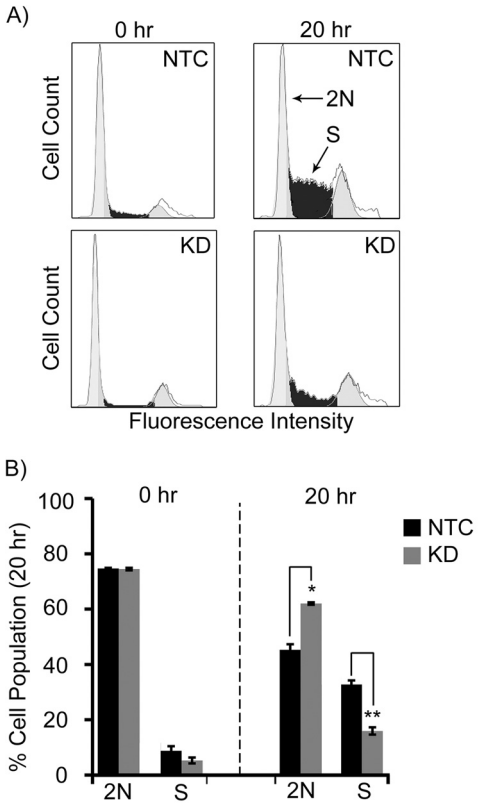

FIGURE 4. **Loss of MGAT4A leads to decreased G_1-S cell cycle progression.** *A*, representative flow cytometry analysis of MCF7-MGAT4A-KD-1 cells or NTC after serum starvation (0 h) followed by 20 h of serum stimulation indicates a slowed 2N (*light gray*) to S phase (*black*) progression in MGAT4A-KD cells. *B*, quantification of % cell population in 2N and S phases for MCF7-MGAT4A-KD-1 (*gray bars*) or NTC (*black bars*), averaged over three biological replicates. *, $p < 0.05$; **, $p < 0.01$ *versus* NTC.

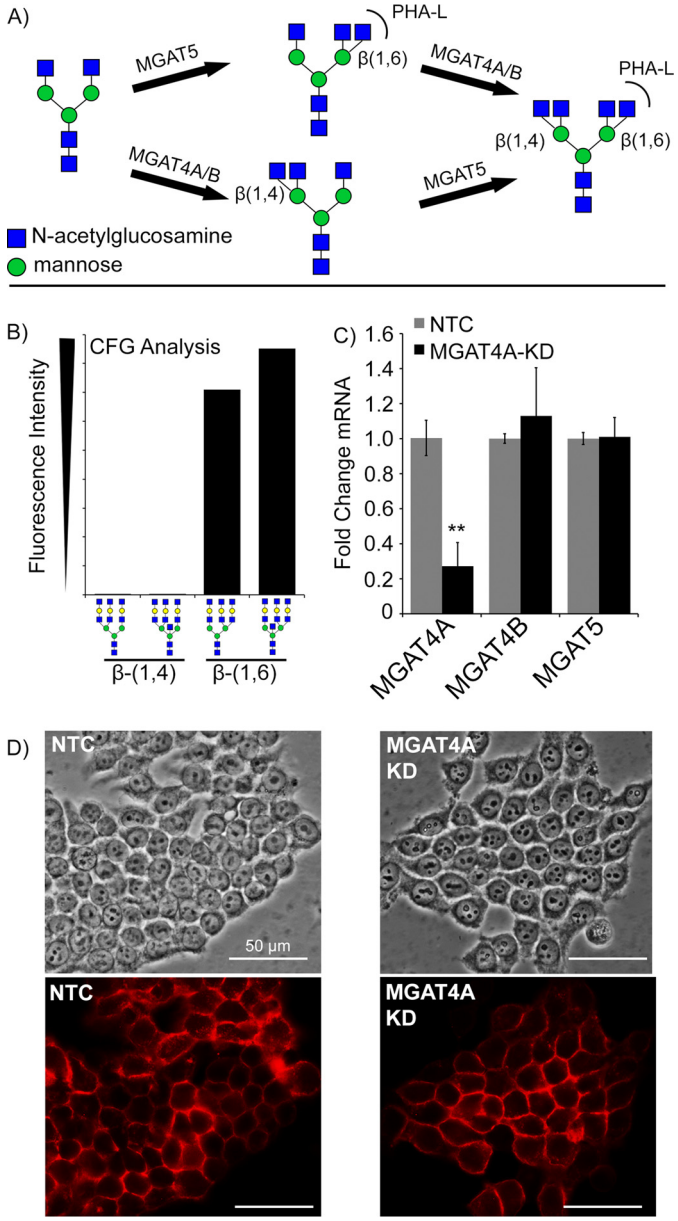

FIGURE 5. **Loss of MGAT4A activity does not affect GlcNAc-β-1,6 branching.** *A*, biosynthetic pathway of tetraantennary branched *N*-glycans. Binding sites of PHA-L are indicated. *B*, analysis of PHA-L binding to the Consortium of Functional Glycomics (*CFG*) glycan array v. 5.0 indicates a preference for GlcNAc-β-1,6 branched products. The graph shows the data for 100 μg/ml biotinylated-PHA-L (Vector Laboratories) binding to glycans bearing only β-1,4 branching (*β-(1,4)*) and the corresponding β-1,6 glycans (*β-(1,6)*). Data are given as fluorescence intensity. *C*, knockdown of MGAT4A in MCF-7 cells shows no significant change in MGAT4B or MGAT5 mRNA levels by qRT-PCR. The graph shows -fold change mRNA expression compared with NTC. $n = 3$ biological replicates. *Error bars* represent the S.D. *D*, fluorescence microscopy of PHA-L stained MGAT4A-KD and NTC cells. No significant loss of PHA-L binding were observed. Images shown are representative of two biological replicates, five images per replicate.

MGAT4A-KD-1 cells was localized to the nucleus, with little cell surface binding observed (Fig. 6*E*, *red channel*). For comparison, we examined the expression of E-cadherin, a noted cell surface marker. Neither the expression (Fig. 6*D*) nor the membrane levels of E-cadherin (Fig. 6*F*) were altered. Although it is unclear whether the change in galectin-3 is important to the cell cycle arrest observed in miR-424 and MGAT4A-KD cells, our data suggest that nuclear galectin-3 may cooperate with miR-424 and MGAT4A in controlling cell cycle progression.

Discussion

Cell cycle progression is controlled by external growth and arrest signals from growth factors and cytokines (Fig. 7). Glycosylation can play a role in mediating such signals through altering the trafficking and sensitivity of cell surface cytokine and growth factor receptors (18, 37–39). MicroRNA, which shapes the identity of a cell through fine-tuned regulation of gene expression, allows us to predict the biological role of specific glycosylation enzymes and the glycans they synthesize (miRNA proxy approach) (8, 9). Herein we demonstrate that miR-424, a cell cycle regulator, targets the 3′-UTR of the glycosylation-related genes MGAT4A, OGT, and GALNT13, suggesting these enzymes may play a role in cell cycle regulation. miRNA can display cell type-dependent effects due to differences in both endogenous miRNA cohorts and gene transcript levels (40). In keeping with this, only MGAT4A, the major enzyme controlling the β-1,4 branch of multiantennary *N*-glycans (32), was targeted by miR-424 in the breast cancer line MCF-7. Regulation of MGAT4A is more pronounced in breast cell lines than in the lung cell line A549 (Fig. 1). Although OGT was not regulated by miR-424 in MCF-7, the miRNA-dependent regulation of OGT is of special interest. Previous analysis of the 3′-UTR of OGT revealed that it is one of the most highly

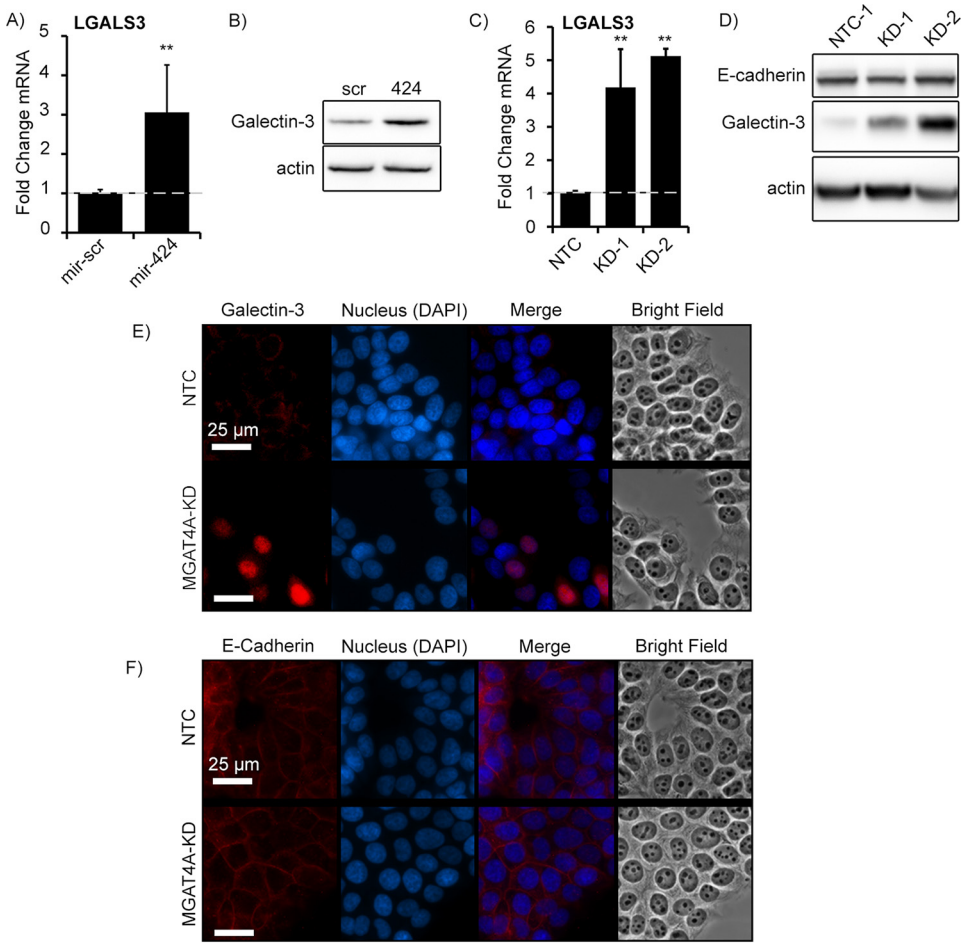

FIGURE 6. **Loss of MGAT4A induces expression and nuclear localization of galectin-3.** *A–D*, MCF-7 cells treated with miR-424 mimic (*A* and *B*) as well as MCF-7-MGAT4A-KD cells (*C* and *D*) show increased LGALS3 (galectin-3) expression by qRT-PCR (*A* and *C*) and Western blot (*B* and *D*) when compared with controls (scrambled mimic (*miR-scr*) and NTC, respectively). **, $p < 0.01$ *versus* miR-scr or NTC. E-cadherin levels are not altered by in MCF-7-MGAT4A-KD cells by Western blot. *D* and *E*, fluorescence microscopy of MGAT4A-KD-1 (*MGAT4A-KD*) MCF-7, or NTC cells stained with α-galectin-3 (*red*) and DAPI (*blue*) indicate significant nuclear localization of galectin-3 in MGAT4A-KD cells. *F*, fluorescence microscopy of MCF7-MGAT4A-KD-1 or NTC cells stained with α-E-cadherin (*red*) and DAPI (*blue*) indicate no change in levels or cell membrane localization of E-cadherin in MGAT4A-KD cells.

regulated glycogenes (41). *O*-GlcNAc, the epitope controlled by this enzyme, is involved in cell proliferation (42, 43), consistent with targeting by miR-424. Thus, further exploration of the interaction between miR-424 and OGT in alternate biological systems is warranted.

miR-424 is up-regulated in normal mammary epithelia in response to TGFβ, a potent inducer of cell cycle arrest (13, 27). Subsequently, miR-424 targets and suppresses a number of cell cycle regulators such as cyclin D1 (CCND1) and CDC25A, resulting in G_1-S phase arrest and slower proliferation (13, 14). Treatment of the normal breast epithelial cell line HMLE with TGFβ caused up-regulation of miR-424 and concomitant down-regulation of MGAT4A and CDC25A (Fig. 2), suggesting that MGAT4A plays a role in this signaling network.

Knockdown of MGAT4A had a profound effect on cell proliferation in multiple breast cell lines (Fig. 3). We observed a decrease in G_1-S progression and a loss of cyclin D1 expression, suggesting arrest of cell cycle progression (Fig. 4). Glycan branching has been previously shown to directly impact cell proliferation mediated by galectin-3 binding to cell surface receptors (44). However, these studies focused on alterations in β-1,6 branched glycans, increases in which first stimulate and then arrest growth rates (18). Knocking down MGAT4A, which biosynthesizes β-1,4 branched glycans, did not affect β-1,6 branched glycans, which are biosynthesized by MGAT5 (Fig. 5). A role for MGAT4A in cell proliferation is supported by work showing MGAT4A is targeted by let-7, a known tumor suppressor (45). This suggests that specific branching patterns (β-1,4 *versus* β-1,6) may play distinct roles, imposing an additional level of control on cell signaling through modulation of glycoproteins such as cytokine and growth factor receptors (Fig. 7).

Both elevated miR-424 and loss of MGAT4A increased expression of galectin-3 (Fig. 6). MCF-7-MGAT4A-KD cells showed a pronounced increase in nuclear galectin-3 by fluorescence microscopy. Nuclear galectin-3 plays a range of biological roles, including manipulation of RNA splicing and enhancement of transcription factor activity (46, 47). Nuclear galectin-3 also plays a role in late-G_1 cell cycle arrest and suppression of anoikis, the programmed cell death in response to loss of cell adhesion (34, 35). Anoikis suppression is observed in migrating metastatic cancer cells and correlates with decreased proliferation (48). Although the specific signaling pathways between β-1,4-branched glycans, cell cycle arrest, and nuclear galectin-3

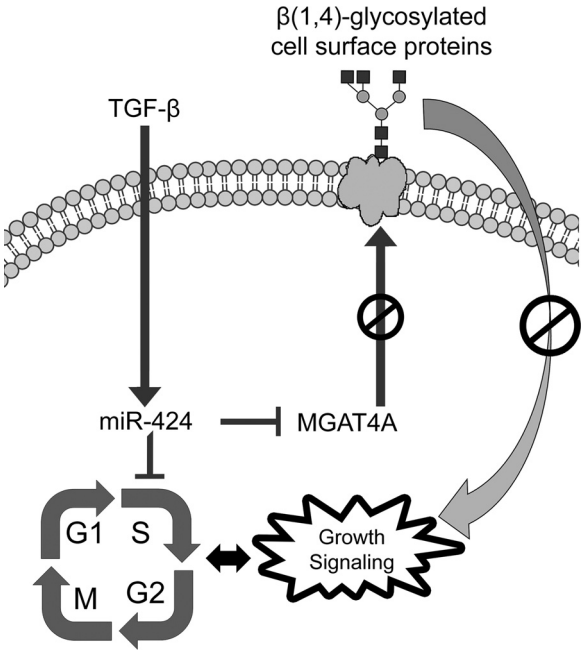

FIGURE 7. **Scheme of the proposed signaling network involving miR-424 and MGAT4A.** MGAT4A synthesizes β-1,4 branched *N*-glycans on glycoproteins (*e.g.* receptors, adhesion molecules). Inhibition of MGAT4A reduces progrowth signaling through glycan-dependent alteration of these glycoproteins. MGAT4A and the direct cell cycle regulators CDC25A and CCND1 are modulated by miR-424, a regulator of cell proliferation.

have not yet been mapped out, our data sheds light on a connection between cell cycle regulation and anoikis suppression of breast epithelial cells in response to changes in specific *N*-glycan branching patterns.

Author Contributions—L. K. M. and C. A. V. designed the experiments, analyzed the data, and wrote the paper. C. A. V. and T. K. performed the experiments.

Acknowledgments—We thank Boval Biosolutions, LLC (Cleburne, Texas) for lyophilized, protease, and IgG-free bovine serum albumin (LY-0081) and Robert Weinberg (Massachusetts Institute of Technology) for the generous gift of HMLE cells.

References

1. Crick, F. (1970) Central dogma of molecular biology. *Nature* 227, 561–563
2. Wahlestedt, C. (2013) Targeting long non-coding RNA to therapeutically up-regulate gene expression. *Nat. Rev. Drug Discov.* 12, 433–446
3. Prabakaran, S., Lippens, G., Steen, H., and Gunawardena, J. (2012) Post-translational modification: nature's escape from genetic imprisonment and the basis for dynamic information encoding. *Wiley Interdiscip. Rev. Syst. Biol. Med.* **4,** 565–583
4. Carthew, R. W., and Sontheimer, E. J. (2009) Origins and mechanisms of miRNAs and siRNAs. *Cell* **136,** 642–655
5. Ameres, S. L., and Zamore, P. D. (2013) Diversifying microRNA sequence and function. *Nat. Rev. Mol. Cell Biol.* **14,** 475–488
6. Schmiedel, J. M., Klemm, S. L., Zheng, Y., Sahay, A., Blüthgen, N., Marks, D. S., and van Oudenaarden, A. (2015) Gene expression. MicroRNA control of protein expression noise. *Science* **348,** 128–132
7. Freeze, H. H., Chong, J. X., Bamshad, M. J., and Ng, B. G. (2014) Solving glycosylation disorders: fundamental approaches reveal complicated pathways. *Am. J. Hum. Genet.* **94,** 161–175
8. Agrawal, P., Kurcon, T., Pilobello, K. T., Rakus, J. F., Koppolu, S., Liu, Z., Batista, B. S., Eng, W. S., Hsu, K. L., Liang, Y., and Mahal, L. K. (2014) Mapping posttranscriptional regulation of the human glycome uncovers microRNA defining the glycocode. *Proc. Natl. Acad. Sci. U.S.A.* **111,** 4338–4343
9. Kurcon, T., Liu, Z., Paradkar, A. V., Vaiana, C. A., Koppolu, S., Agrawal, P., and Mahal, L. K. (2015) miRNA proxy approach reveals hidden functions of glycosylation. *Proc. Natl. Acad. Sci. U.S.A.* **112,** 7327–7332
10. Finnerty, J. R., Wang, W. X., Hébert, S. S., Wilfred, B. R., Mao, G., and Nelson, P. T. (2010) The miR-15/107 group of microRNA genes: evolutionary biology, cellular functions, and roles in human diseases. *J. Mol. Biol.* **402,** 491–509
11. Kozomara, A., and Griffiths-Jones, S. (2011) miRBase: integrating microRNA annotation and deep-sequencing data. *Nucleic Acids Res.* **39,** D152–D157
12. Llobet-Navas, D., Rodríguez-Barrueco, R., Castro, V., Ugalde, A. P., Sumazin, P., Jacob-Sendler, D., Demircan, B., Castillo-Martín, M., Putcha, P., Marshall, N., Villagrasa, P., Chan, J., Sanchez-Garcia, F., Pe'er, D., Rabadán, R., Iavarone, A., Cordón-Cardó, C., Califano, A., López-Otín, C., Ezhkova, E., and Silva, J. M. (2014) The miR-424(322)/503 cluster orchestrates remodeling of the epithelium in the involuting mammary gland. *Genes Dev.* **28,** 765–782
13. Llobet-Navas, D., Rodriguez-Barrueco, R., de la Iglesia-Vicente, J., Olivan, M., Castro, V., Saucedo-Cuevas, L., Marshall, N., Putcha, P., Castillo-Martin, M., Bardot, E., Ezhkova, E., Iavarone, A., Cordon-Cardo, C., and Silva, J. M. (2014) The microRNA 424/503 cluster reduces CDC25A expression during cell cycle arrest imposed by transforming growth factor β in mammary epithelial cells. *Mol. Cell. Biol.* **34,** 4216–4231
14. Liu, Q., Fu, H., Sun, F., Zhang, H., Tie, Y., Zhu, J., Xing, R., Sun, Z., and Zheng, X. (2008) miR-16 family induces cell cycle arrest by regulating multiple cell cycle genes. *Nucleic Acids Res.* **36,** 5391–5404
15. Hart, G. W., and Copeland, R. J. (2010) Glycomics hits the big time. *Cell* **143,** 672–676
16. Abdel Rahman, A. M., Ryczko, M., Nakano, M., Pawling, J., Rodrigues, T., Johswich, A., Taniguchi, N., and Dennis, J. W. (2015) Golgi *N*-glycan branching *N*-acetylglucosaminyltransferases I, V, and VI promote nutrient uptake and metabolism. *Glycobiology* **25,** 225–240
17. Slawson, C., Zachara, N. E., Vosseller, K., Cheung, W. D., Lane, M. D., and Hart, G. W. (2005) Perturbations in O-linked β-*N*-acetylglucosamine protein modification cause severe defects in mitotic progression and cytokinesis. *J. Biol. Chem.* **280,** 32944–32956
18. Lau, K. S., Partridge, E. A., Grigorian, A., Silvescu, C. I., Reinhold, V. N., Demetriou, M., and Dennis, J. W. (2007) Complex *N*-glycan number and degree of branching cooperate to regulate cell proliferation and differentiation. *Cell* **129,** 123–134
19. Carlberg, M., and Larsson, O. (1993) Role of *N*-linked glycosylation in cell-cycle progression and initiation of DNA synthesis in tumor-transformed human fibroblasts. *Anticancer Res.* **13,** 167–171
20. Partridge, E. A., Le Roy, C., Di Guglielmo, G. M., Pawling, J., Cheung, P., Granovsky, M., Nabi, I. R., Wrana, J. L., and Dennis, J. W. (2004) Regulation of cytokine receptors by Golgi *N*-glycan processing and endocytosis. *Science* **306,** 120–124
21. Sakabe, K., and Hart, G. W. (2010) *O*-GlcNAc transferase regulates mitotic chromatin dynamics. *J. Biol. Chem.* **285,** 34460–34468
22. Elenbaas, B., Spirio, L., Koerner, F., Fleming, M. D., Zimonjic, D. B., Donaher, J. L., Popescu, N. C., Hahn, W. C., and Weinberg, R. A. (2001) Human breast cancer cells generated by oncogenic transformation of primary mammary epithelial cells. *Genes Dev.* **15,** 50–65
23. Mani, S. A., Guo, W., Liao, M. J., Eaton, E. N., Ayyanan, A., Zhou, A. Y., Brooks, M., Reinhard, F., Zhang, C. C., Shipitsin, M., Campbell, L. L., Polyak, K., Brisken, C., Yang, J., and Weinberg, R. A. (2008) The epithelial-mesenchymal transition generates cells with properties of stem cells. *Cell* **133,** 704–715
24. Livak, K. J., and Schmittgen, T. D. (2001) Analysis of relative gene expression data using real-time quantitative PCR and the 2(−ΔΔCt) method. *Methods* **25,** 402–408
25. Betel, D., Koppal, A., Agius, P., Sander, C., and Leslie, C. (2010) Comprehensive modeling of microRNA targets predicts functional non-conserved and non-canonical sites. *Genome Biol.* **11,** R90
26. Betel, D., Wilson, M., Gabow, A., Marks, D. S., and Sander, C. (2008) The

microRNA.org resource: targets and expression. *Nucleic Acids Res.* **36,** D149–D153
27. Massagué, J. (2012) TGFβ signalling in context. *Nat. Rev. Mol. Cell Biol.* **13,** 616–630
28. Crissman, H. A., and Steinkamp, J. A. (1973) Rapid, simultaneous measurement of DNA, protein, and cell volume in single cells from large mammalian cell populations. *J. Cell Biol.* **59,** 766–771
29. Takamatsu, S., Antonopoulos, A., Ohtsubo, K., Ditto, D., Chiba, Y., Le, D. T., Morris, H. R., Haslam, S. M., Dell, A., Marth, J. D., and Taniguchi, N. (2010) Physiological and glycomic characterization of *N*-acetylglucosaminyltransferase-IVa and -IVb double deficient mice. *Glycobiology* **20,** 485–497
30. Schachter, H. (1986) Biosynthetic controls that determine the branching and microheterogeneity of protein-bound oligosaccharides. *Biochem. Cell Biol.* **64,** 163–181
31. Cummings, R. D., and Kornfeld, S. (1982) Characterization of the structural determinants required for the high affinity interaction of asparagine-linked oligosaccharides with immobilized *Phaseolus vulgaris* leukoagglutinating and erythroagglutinating lectins. *J. Biol. Chem.* **257,** 11230–11234
32. Ohtsubo, K., Takamatsu, S., Minowa, M. T., Yoshida, A., Takeuchi, M., and Marth, J. D. (2005) Dietary and genetic control of glucose transporter 2 glycosylation promotes insulin secretion in suppressing diabetes. *Cell* **123,** 1307–1321
33. Oguri, S., Yoshida, A., Minowa, M. T., and Takeuchi, M. (2006) Kinetic properties and substrate specificities of two recombinant human *N*-acetylglucosaminyltransferase-IV isozymes. *Glycoconj. J.* **23,** 473–480
34. Kim, H. R., Lin, H. M., Biliran, H., and Raz, A. (1999) Cell cycle arrest and inhibition of anoikis by galectin-3 in human breast epithelial cells. *Cancer Res.* **59,** 4148–4154
35. Yoshii, T., Fukumori, T., Honjo, Y., Inohara, H., Kim, H. R., and Raz, A. (2002) Galectin-3 phosphorylation is required for its anti-apoptotic function and cell cycle arrest. *J. Biol. Chem.* **277,** 6852–6857
36. Shimura, T., Takenaka, Y., Fukumori, T., Tsutsumi, S., Okada, K., Hogan, V., Kikuchi, A., Kuwano, H., and Raz, A. (2005) Implication of galectin-3 in Wnt signaling. *Cancer Res.* **65,** 3535–3537
37. Walsh, S. T. (2010) A biosensor study indicating that entropy, electrostatics, and receptor glycosylation drive the binding interaction between interleukin-7 and its receptor. *Biochemistry* **49,** 8766–8778
38. Takeuchi, Y., Morise, J., Morita, I., Takematsu, H., and Oka, S. (2015) Role of site-specific *N*-glycans expressed on GluA2 in the regulation of cell surface expression of AMPA-type glutamate receptors. *PLoS ONE* **10,** e0135644
39. Zhou, R. W., Mkhikian, H., Grigorian, A., Hong, A., Chen, D., Arakelyan, A., and Demetriou, M. (2014) *N*-Glycosylation bidirectionally extends the boundaries of thymocyte positive selection by decoupling Lck from Ca^{2+} signaling. *Nat. Immunol.* **15,** 1038–1045
40. Kuhn, D. E., Martin, M. M., Feldman, D. S., Terry, A. V., Jr., Nuovo, G. J., and Elton, T. S. (2008) Experimental validation of miRNA targets. *Methods* **44,** 47–54
41. Kasper, B. T., Koppolu, S., and Mahal, L. K. (2014) Insights into miRNA regulation of the human glycome. *Biochem. Biophys. Res. Commun.* **445,** 774–779
42. Bullen, J. W., Balsbaugh, J. L., Chanda, D., Shabanowitz, J., Hunt, D. F., Neumann, D., and Hart, G. W. (2014) Cross-talk between two essential nutrient-sensitive enzymes: *O*-GlcNAc transferase (OGT) and AMP-activated protein kinase (AMPK). *J. Biol. Chem.* **289,** 10592–10606
43. Barnes, J. W., Tian, L., Heresi, G. A., Farver, C. F., Asosingh, K., Comhair, S. A., Aulak, K. S., and Dweik, R. A. (2015) *O*-Linked β-*N*-acetylglucosamine transferase directs cell proliferation in idiopathic pulmonary arterial hypertension. *Circulation* **131,** 1260–1268
44. Boscher, C., Zheng, Y. Z., Lakshminarayan, R., Johannes, L., Dennis, J. W., Foster, L. J., and Nabi, I. R. (2012) Galectin-3 protein regulates mobility of *N*-cadherin and GM1 ganglioside at cell-cell junctions of mammary carcinoma cells. *J. Biol. Chem.* **287,** 32940–32952
45. Guo, Y., Li, S., Qu, J., Ye, L., Wang, S., Fan, J., Wang, Q., and Zhang, J. (2014) Let-7c inhibits metastatic ability of mouse hepatocarcinoma cells via targeting mannoside acetylglucosaminyltransferase 4 isoenzyme A. *Int. J. Biochem. Cell Biol.* **53,** 1–8
46. Dagher, S. F., Wang, J. L., and Patterson, R. J. (1995) Identification of galectin-3 as a factor in pre-mRNA splicing. *Proc. Natl. Acad. Sci. U.S.A.* **92,** 1213–1217
47. Newlaczyl, A. U., and Yu, L. G. (2011) Galectin-3: a jack-of-all-trades in cancer. *Cancer Lett.* **313,** 123–128
48. Smit, M. A., Geiger, T. R., Song, J. Y., Gitelman, I., and Peeper, D. S. (2009) A Twist-Snail axis critical for TrkB-induced epithelial-mesenchymal transition-like transformation, anoikis resistance, and metastasis. *Mol. Cell. Biol.* **29,** 3722–3737